Applied Physics Letters ARTICLE scitation.org/journal/apl

Label-free deeply subwavelength optical microscopy

Cite as: Appl. Phys. Lett. **116**, 131105 (2020); doi: 10.1063/5.0003330
Submitted: 31 January 2020 · Accepted: 12 March 2020 ·
Published Online: 31 March 2020

T. Pu,[1,a)] J. Y. Ou,[1] N. Papasimakis,[1,b)] and N. I. Zheludev[1,2,c)]

AFFILIATIONS

[1]Optoelectronics Research Centre and Centre for Photonic Metamaterials, University of Southampton, Southampton SO17 1BJ, United Kingdom
[2]Centre for Disruptive Photonic Technologies, The Photonics Institute, School of Physical and Mathematical Sciences, Nanyang Technological University, 637371 Singapore

[a)]On leave from: Key Laboratory of Microelectronics Devices and Integrated Technology, Institute of Microelectronics, Chinese Academy of Sciences, Beijing 100029, China.
[b)]**Author to whom correspondence should be addressed:** n.papasimakis@soton.ac.uk
[c)]zheludev@soton.ac.uk

ABSTRACT

We report the experimental demonstration of deeply subwavelength far-field optical microscopy of unlabeled samples. We beat the $\sim\lambda/2$ diffraction limit of conventional optical microscopy several times over by recording the intensity pattern of coherent light scattered from the object into the far-field. We retrieve information about the object with a deep learning neural network trained on scattering events from a large set of known objects. The microscopy retrieves dimensions of the imaged object probabilistically. Widths of the subwavelength components of the dimer are measured with a precision of $\lambda/10$ with the probability higher than 95% and with a precision of $\lambda/20$ with the probability better than 77%. We argue that the reported microscopy can be extended to objects of random shape and shall be particularly efficient on object of known shapes, such as found in routine tasks of machine vision, smart manufacturing, and particle counting for life sciences applications.

The ability to image at the nanometer scale using visible light remains a long-standing fundamental challenge for optics. Despite over 400 years of developments in microscopy, subwavelength optical imaging is only possible through the use of near-field probes[1] or fluorescent labels.[2,3] Moreover, combining the latter with artificial intelligence approaches has been shown to improve imaging resolution.[4,5] However, fluorescence-based and near-field methods exclude many applications. Several other techniques have been developed to break through the "diffraction limit" of conventional microscopes,[6–8] which, however, led only to modest enhancement of resolution in far-field techniques.[9,10]

The distinction between far-field and near-field imaging techniques is important. In the context of imaging, the near-field and far-field zones are regions of the electromagnetic field around an object, resulting from radiation scattering on the object. The near-field consists of non-propagating (evanescent) components with the wavevector larger than that of free-space propagating light waves. These non-propagating field components exponentially decay within a distance of a wavelength from the object. Detecting the near-field is possible by converting non-propagating components into propagating ones by placing a small probe in the proximity of the object. Such detection is used in high-resolution scanning near-field microscopy (SNOM). However, SNOM is intrusive and does not allow imaging inside the object. For that reason, imaging techniques that rely only on propagating components of the scattered field are of considerable interest for many applications in nanotechnology and biology.

In our recent theoretical paper,[11] we introduced a type of microscopy, which reveals the fine structure of a physical object through its far-field intensity scattering pattern under illumination by either a coherent plane wave or topological superoscillatory coherent light. We have shown that reconstruction of the object can be achieved by machine learning using a neural network trained on a large number of scattering events on known objects. In this earlier paper, we demonstrated computationally that resolution far beyond the conventional diffraction limit should be possible with either plane waves or superoscillatory illumination, with higher resolution being achievable in the latter case. In computer modeling experiments, a dimer comprising

two subwavelength opaque particles was imaged with a resolution exceeding $\lambda/200$.

Here, we report the first proof-of-principle laboratory experiment, confirming that this imaging technique can provide deeply subwavelength resolution. Using plane wave illumination, we imaged a dimer sample cut in an opaque metallic film comprising a pair of nanometer scale slits of unknown width and spacing between them.

In practical terms, the main challenge in the implementation of deeply subwavelength optical microscopy is creating a reliable and trustworthy training set for deep learning. Such a dataset can be either virtual or physical. The virtual training dataset of imaged objects and their diffraction scattering patterns can be generated by numerical modeling (Maxwell solving) on a random set of *a priori* defined large set of random virtual training objects. Here, the main challenge is to ensure that the computer model is meticulously congruent with the physical realization of the microscope to allow adequate imaging of the real object, which may be problematic. Alternatively, a physical dataset can be created by fabricating a number of real scattering elements followed by recording of their scattering patterns in the imaging instrument. Generating a physical set is labor-intensive, but such a set is naturally congruent with the imaging microscope. The choice of the training dataset (physical or virtual) shall be made with the desired resolution and complexity of the microscope optical tract, and, in general, higher resolution would require large training datasets.

Another challenge in implementing deeply subwavelength optical microscopy is in registering diffraction patterns with high spatial resolution. However, since the diffracted field reaching the image sensor is formed by free-space propagating waves, it can be imaged at any magnification without the loss of resolution by adjusting the magnification level necessary to ensure that the detector pixels are smaller than the required resolution. Moreover, our analysis shows that the reconstruction of the scattering object by the deep learning neural network is tolerant to the dynamic range of the detector with the dynamic range of 40 dB being sufficient for deeply subwavelength imaging. However, narrow-band coherent laser radiation shall be used to ensure the distinguishability of the diffraction patterns of different objects. Therefore, conventional microscopy hardware with minor modifications can be used for proof-of-principle demonstrations of the deeply subwavelength optical microscopy described above.

Our experiments were performed in a commercial dual optical microscope. The imaging target was placed on the imaging plane of the apparatus and illuminated with a laser diode at the wavelength of $\lambda = 795$ nm through a low numerical aperture lens. Light diffracted on the dimer was then imaged at a distance of $h = 2\lambda$ from the image plane by a high-numerical lens with a 6× magnification changer and a 5.5-MP sCMOS camera, see Fig. 1. The imaging system of our apparatus had a magnification of 600 corresponding to an effective pixel size of 10.8 nm on the image plane. The imaged dimer, placed in the center of view, is characterized by the width of the two slits, A and C, and the separation, B, between the two slits (edge-to-edge) [see Fig. 1(d)].

Dimensions of the unknown dimer are retrieved with a deep learning neural network trained on a set of scattering events from dimers of known dimensions. We chose to use a physical training set of only 100 dimers, which, in our modeling, was sufficient to achieve resolution beyond $\lambda/10$. For that matter, we fabricated a set of 144 dimer slits of random size by focused ion milling on a 40 nm thick chromium film deposited on a glass substrate, see the SEM image of

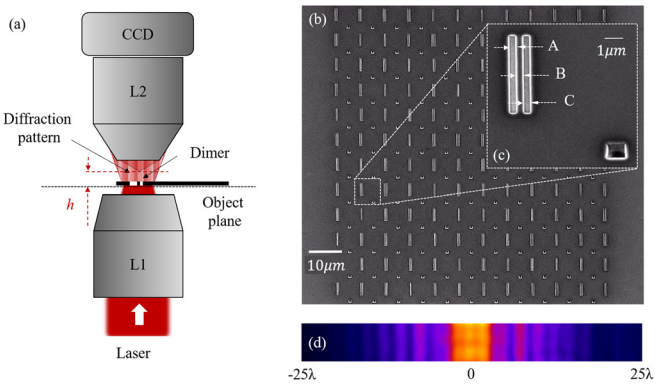

FIG. 1. Imaging apparatus and the physical training set. The dimer to be imaged is placed on the object plane and is illuminated by a coherent laser light source at the wavelength of $\lambda = 795$ nm through a low numerical aperture lens L1 (NA = 0.3). The light diffracted on the dimer is imaged at a distance $h = 2\lambda$ from the dimer by a high numerical aperture lens L2 (NA = 0.9) (a). The set of $12 \times 12 = 144$ dimer slits is fabricated by focused ion milling on a chromium film on the glass substrate (b); slits of the dimers have random widths A and C and are randomly spaced by distance B. A square alignment mark is fabricated near each dimer (c). The intensity pattern of coherent light diffracted on each dimer is recorded. Plate (d) shows a characteristic diffraction pattern of a dimer in a field of view 50λ wide.

the set in Fig. 2(a). In the set, parameters A, B, and C of the dimer were randomly chosen in the interval from 0.1λ to 0.6λ (80 nm to 477 nm). Here, almost all dimer dimensions in the set are well beyond the $\lambda/2$ diffraction limit, and hence, their inner structure would be beyond the diffraction limit of conventional microscopy.

Upon fabrication, the dimers were measured to nanometer precision using a scanning electron microscope. One hundred dimers from this set were used for network training, while the rest were used as imaged objects of unknown dimensions in the test microscopy experiments. The diffraction patterns from the set of one hundred dimers were recorded in the imaging apparatus and mutually aligned using a position mark fabricated near each dimer. To increase accuracy, the 2D SEM images of the dimers and their diffraction patterns were averaged along the length of the slits [vertical axis in Fig. 1(b)]. The diffraction patterns, together with their dimensions measured by the SEM, formed the physical training set for the neural network.

The neural network consisted of four fully connected layers with 128, 512, 256, and 3 neurons [see Fig. 2(c)]. The first three layers were activated by the Rectified Linear Unit (ReLU) activation function, while the last layer is activated by the sigmoid function. To avoid over-fitting, dropout layers with a rate of 20% are inserted after each of the first three layers. The network was trained using the Adam stochastic optimization method, and the mean absolute error loss function was monitored.

Upon completion of the training with 100 random dimers of *a priori* known sizes, the apparatus was ready for imaging dimers of unknown size. To quantify the effect of the relatively small size of the training dataset on the imaging process, we repeated the training process 500 times randomizing the training set. We have applied the 500 different realizations of the trained network in imaging unknown dimers, which resulted in a distribution of 500 retrieved values for each parameter (A, B, and C) of each dimer. We have undertaken a statistical analysis of the distributions of retrieved values to determine the resolution of microscopy.

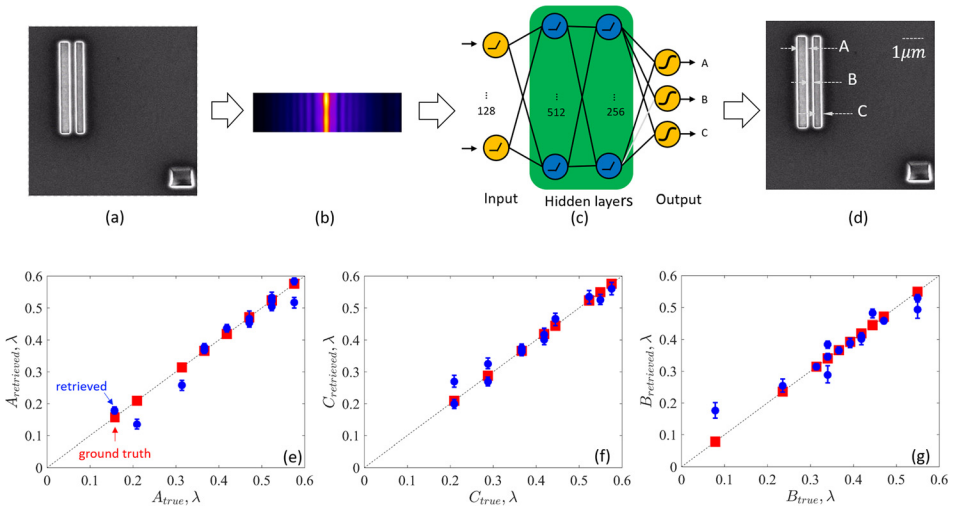

FIG. 2. Imaging of unknown dimers. The intensity profile of the diffraction pattern (b) of an unknown dimer (a) is recorded. Dimensions A, B, and C of the dimer are retrieved from the diffraction pattern by the trained neural network (c). Plates (e)–(g) present comparisons of the retrieved dimensions A (e), C (f), and B (g) of the dimers vs the true dimensions. The true dimensions (red squares) are measured using a scanning electron microscope for a set of N = 14 measurements. The retrieved dimensions are evaluated for 500 different trained networks, resulting in a distribution of retrieved values. Red squares represent the ground truth values of A, B, and C dimensions, while blue circles correspond to the median predicted values. The blue error bars indicate the interquartile range of the distribution of predicted values. The dimers in this series are "unseen": they are of random size and have not been used in the network training process.

The results of our experiments on 14 randomly selected dimers of unknown dimensions are presented in Figs. 2(e)–2(g), where the retrieved values (blue circles) are plotted as a function of the true dimensions. Here, the dashed black line represents perfect imaging, while dispersion of the points away from it indicates a divergence between the true and retrieved values. For all three dimensions of the dimers (A, B, and C), we observe that the retrieved values closely follow the true value, which slightly diverge for the smallest values. To quantify the resolution of imaging, we calculated the interquartile range (IQR) of the distribution of retrieved values for each one of the 14 unknown dimers [see error bars in Figs. 2(e)–2(g)]. We observed that the stochastic errors introduced by the network training process do not exhibit a strong dependence on the dimer feature sizes.

The deeply subwavelength optical microscopy reported here retrieves dimer's parameters probabilistically. Therefore, resolution of the technique shall be assessed from the point of view of how likely a measured value is equal to the real value within the claimed resolution. This can be easily evaluated from the distribution of retrieved values for the measured dimers: the probability of retrieving individual dimensions A and C with a precision of $\lambda/10$ is better than 95%. The same parameters are retrieved with a precision of $\lambda/20$ with the probability better than 77%. The dimer gap is be resolved with a precision of $\lambda/10$ with the probability of 87% and with a precision of $\lambda/20$ in 70% of cases.

The experimentally observed resolution considerably exceeds the $\lambda/2$ diffraction limit of conventional optical microscopes. We, therefore, argue that the deep learning process involving a neural network trained on *a priori* known objects creates a powerful and accurate deconvolution mechanism, while sparsity and prior knowledge about the object help the retrieval process, similar to how sparsity helps "blind" compressed sensing techniques. Remarkably, such resolution is achieved with a small physical dataset comprising just 100 dimers. We expect that imaging more complex objects will require increasingly larger datasets. Moreover, we argue that larger training datasets will allow us to boost the resolution enhancement by at least another order of magnitude[11] reaching the molecular resolution.

In conclusion, we have experimentally demonstrated far-field deeply subwavelength optical microscopy of unlabeled samples, which employs artificial intelligence to retrieve, with resolution exceeding $\lambda/10$, parameters of a physical object from its scattering pattern. Although so far, we demonstrate the concept for one-dimensional imaging, it can be extended to two- and three-dimensional objects, as well as objects of *a priori* unknown shape. We expect that much higher resolution shall be possible with topological superoscillatory illumination as it will ensure much higher discrimination of small features of the imaged object by the pattern of scattered light than conventional illumination.

Finally, for centuries, imaging was a technique of representation of an object's form by creating a light pattern resembling the object, in the way that a conventional microscope creates it on the retina of the observer's eye or a screen. The proliferation of computers and image processing techniques has often replaced the light pattern representation by patterns on the computer screen or data stored in the computer memory. This is now common practice in modern optical imaging techniques, such as confocal imaging, SNOM, and Stimulated Emission Depletion Microscopy (STED), as well as for most of the electron-beam imaging techniques. We argue that the technique described in this work is a computer-enabled imaging technique that provides a comprehensive representation of the object's form including all its dimensions and allows full reconstruction of its shape (see the contemporary definition of imaging in Ref. 12). Our technique is also a form of microscopy according to the common definition of microscopy as "the technical field of using microscopes to view objects … that cannot be seen with the naked eye (objects that are not within the resolution range of the normal eye)."[13]

The authors acknowledge the support of the Singapore Ministry of Education (Grant No. MOE2016-T3-1-006), the Agency for Science, Technology and Research (A*STAR) Singapore (Grant No. SERC A1685b0005), the Engineering and Physical Sciences Research Council UK (Grant Nos. EP/N00762X/1 and EP/M009122/1), and the European Research Council (Advanced Grant No. FLEET-786851). T.P. acknowledges the support of the Chinese Scholarship Council (CSC No. 201804910540). Following a period of embargo, the data from this paper can be obtained from the University of Southampton ePrints research repository (https://doi.org/10.5258/SOTON/D1301).

REFERENCES

[1]F. Keilman and R. Hillenbrand, "Near-field microscopy by elastic light scattering from a tip," Philos. Trans. R. Soc. London, Ser. A **362**, 787–805 (2004).
[2]M. Fernandez-Suarez and A. Y. Ting, "Fluorescent probes for super-resolution imaging in living cells," Nat. Rev. Mol. Cell Biol. **9**, 929 (2008).
[3]A. Cornea and P. M. Conn, *Fluorescence Microscopy: Super-Resolution and Other Novel Techniques* (Elsevier, 2014).
[4]H. Wang, Y. Rivenson, Y. Jin, Z. Wei, R. Gao, H. Günaydın, L. A. Bentolila, C. Kural, and A. Ozcan, "Deep learning enables cross-modality super-resolution in fluorescence microscopy," Nat. Methods **16**, 103–110 (2019).
[5]C. Belthangady and L. A. Royer, "Applications, promises, and pitfalls of deep learning for fluorescence image reconstruction," Nat. Methods **16**, 1215–1225 (2019).
[6]W. Lukosz, "Optical systems with resolving powers exceeding the classical limit," J. Opt. Soc. Am. **56**, 1463–1471 (1966).
[7]J. Qin, "Fourier domain optical tool normalization for quantitative parametric image reconstruction," Appl. Opt. **52**, 6512 (2013).
[8]E. Narimanov, "Resolution limit of label-free far-field microscopy," Adv. Photonics **1**, 056003 (2019).
[9]E. T. F. Rogers, J. Lindberg, T. Roy, S. Savo, J. E. Chad, M. R. Dennis, and N. I. Zheludev, "A super-oscillatory lens optical microscope for subwavelength imaging," Nat. Mater. **11**, 432 (2012).
[10]G. Yuan, K. S. Rogers, E. T. F. Rogers, and N. I. Zheludev, "Far-field superoscillatory metamaterial superlens," Phys. Rev. Appl. **11**, 064016 (2019).
[11]T. Pu, V. Savinov, G. Yuan, N. Papasimakis, and N. I. Zheludev, "Unlabelled far-field deeply subwavelength superoscillatory imaging (DSSI)," arXiv:1908.00946 (2019).
[12]See https://en.wikipedia.org/wiki/Imaging for a contemporary definition of imaging.
[13]See https://en.wikipedia.org/wiki/Microscopy for definition of microscopy.